Updating active deformation inventory maps in mining areas by integrating InSAR with LiDAR datasets

Liuru Hu[1,2,3], Roberto Tomás [1], Xinming Tang[2], Juan López Vinielles[4], Gerardo Herrera[4], Tao Li[2]

(1) Universidad de Alicante, Dpto. de Ingeniería Civil, Alicante, Spain.
(2) Land Satellite Remote Sensing Application Center (LASAC), Ministry of Natural Resources of P.R. China, Beijing, China.
(3) The First Topographic Surveying Brigade of Ministry of Natural Resources of the People's Republic of China, Xi'an, China.
(4) Geological Survey of Spain (IGME -CSIC), Geohazards and Climate Change Department, Geohazards InSAR Laboratory and Modeling Group (InSARlab), Madrid, Spain.

ESA-MOST Dragon Cooperation
2022 DRAGON 5 MID-TERM RESULTS SYMPOSIUM
17-21 October 2022 | Online Event

ABSTRACT

This work illustrates the potential of exploiting space-borne InSAR and airborne LiDAR techniques, combined with data inferred through safety factor maps, to obtain and update inventory maps of active deformations in mining areas. The proposed approach is illustrated by analyzing the region of Sierra de Cartagena-La Union (Murcia), a mountainous mining area in the southeast Spain. The results highlight the effectiveness of different remote sensing techniques (i.e., InSAR and LiDAR) jointly with classical methods and simple geotechnical models for slope stability evaluation to update inventory maps of active deformation areas in mining areas.

INTRODUCTION

The Sierra de Cartagena-La Union (Murcia) has been intensively exploited since the Roman period as a metal mining area. Previous studies have addressed some issues related to the study of active deformation areas such as stability of abandoned open pit mines, the mapping of ground movements and mining subsidence in specific areas of the Sierra de Cartagena-La Union.

Ground surface motions in mining areas are usually monitored using surface and subsurface techniques (e.g. surveying, settlement cells or inclinometers) which require in situ measurements and represent a costly solution. Optical remote sensing is highly susceptible to external factors such as the subjective opinions of experts and very time consuming. Alternatively, Interferometric Synthetic Aperture Radar (InSAR) is a good technique for the detection, the delineation of boundaries, and the assessment of ADAs. Multi-temporal LiDAR (Light Detection and Ranging) datasets used to produce an inventory map not only is conductive to a loss of resolution, but also allows better capture of subtle changes on quick deformation.

OBJECTIVE

- To update the existing active deformation areas (ADAs) in Sierra de Cartagena-La Union (Murcia)
- To propose a comprehensive systematic methodology for the identification and classification of ADAs
- To apply LiDAR as a complementary technique for the updating of active areas

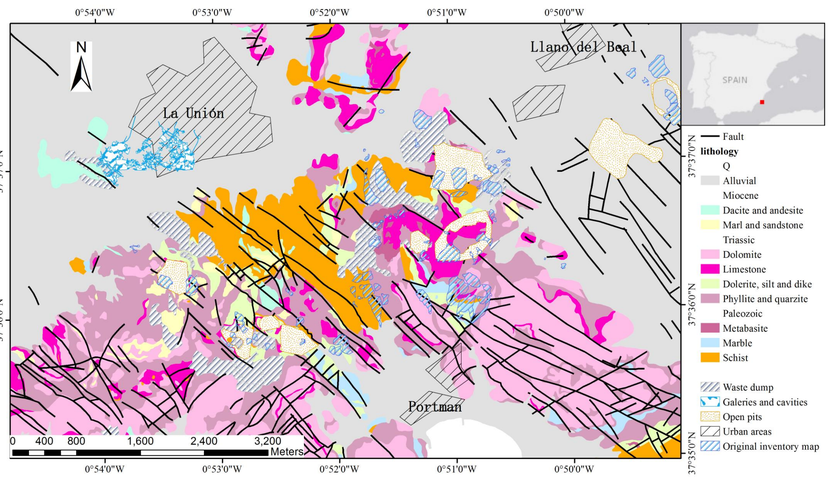

Fig. 1. Geological map of study area.

METHODS

The methodology relies on the joint exploitation of InSAR, LiDAR and safety factor maps, to update inventory maps. Firstly, the ascending and descending Line of Sight (LOS) displacement velocity maps were derived using StaMPS PSI-InSAR processing chain, which was then decomposed into horizontal (east-west) and vertical velocity maps by the app LOS2HV from ADATools. Secondly, LiDAR-derived velocity was calculated comparing both available point clouds with the multiscale model-to-model cloud comparison (M3C2) algorithm. Third, active deformation areas (ADAs) were automatically mapped using the app of ADAfinder from ADATools. At the same time, the infinite slope stability model, a simplistic slope stability model that can be easily applied using geographical information systems on a regional scale, was employed to perform stability analyses of the whole study region to obtain the safety factor map. Finally, the inventory map was updated by probability method (frequency ratio) and susceptibility degree, and cross analysis different ADAs by confusion matrix.

RESULTS

Four InSAR velocity maps were used to identify the Active Deformation Areas (i.e. ADA_D, ADA_A, ADA_H and ADA_V) by ADAfinder using the same rate threshold (i.e. 3 mm/year). The preliminary movement range was roughly portrayed by the four InSAR ADAs maps. ADA_L were derived from LiDAR results. As shown in Figures 5 and 6, the average SF is considerably reduced when H_W =1 and the total unstable area (i.e. that exhibiting a SF<1) is much greater than that calculated for H_W =0.

A joint active level inventory map was separated into 137 ADAs, including 1 for level 6, 5 for level 5, 16 for level 4, 27 for level 3, 23 for level 2 and 63 for level 1.

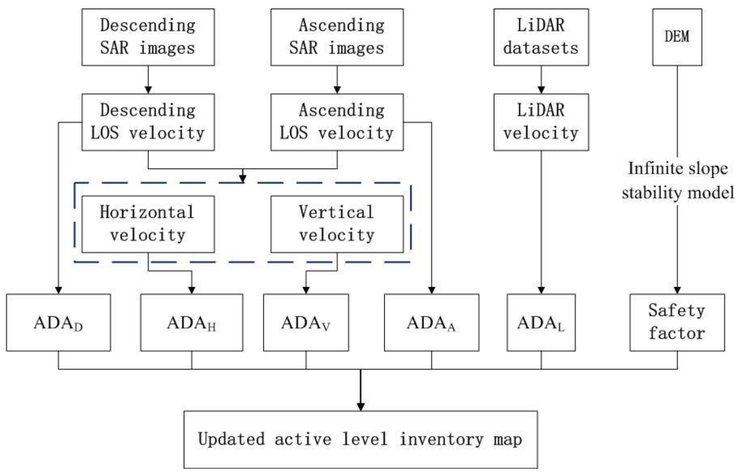

Fig. 2. The proposed flowchart to update active deformation areas inventory map.

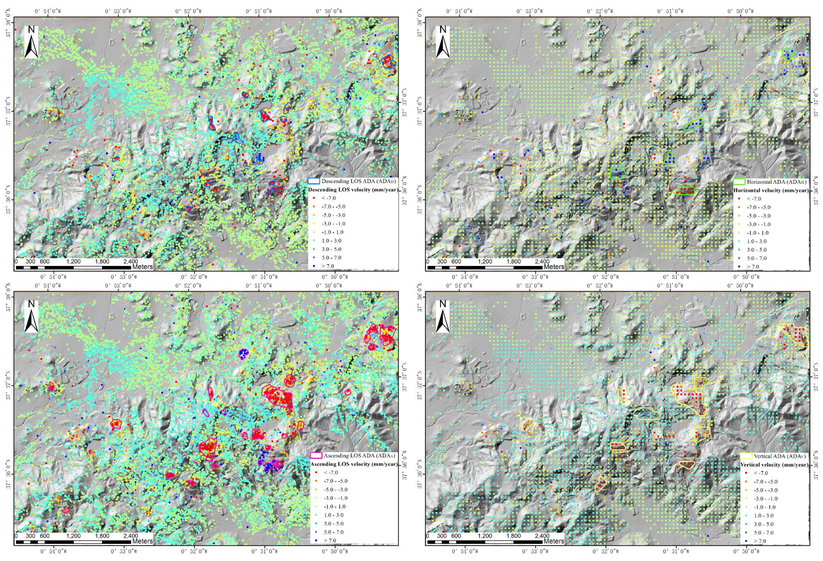

Fig. 3. Descending LOS velocity map, ascending LOS velocity map, horizontal east-west displacement velocity map, vertical displacement velocity map for the period from October 2016 to November 2021. The blue, purple, green, yellow solid polygons indicate the boundaries of the descending LOS ADA (ADA_D), ascending LOS ADA (ADA_A), horizontal ADA (ADA_H), vertical ADA (ADA_V).

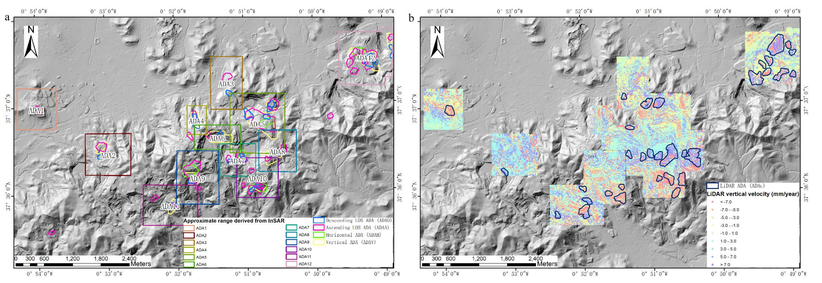

Fig. 4. (a) The approximate range derived from descending (ADA_D), ascending (ADA_A), horizontal (ADA_H) and vertical (ADA_V) ADAs. The labels indicate the mark number of the detected ADAs. (b) LiDAR vertical velocity map for the period from 2009 to 2016. The black solid polygons indicate the boundaries of the LiDAR ADA (ADA_L).

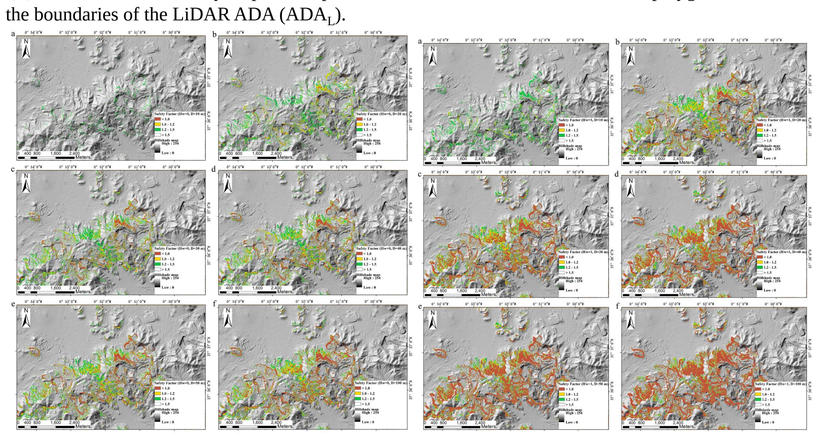

Fig. 5. Map of the safety factor for Hw=0 for depth values of the slip surface (D) varying from 10 to 100 m computed by the infinite slope model..

Fig. 6. Map of the safety factor for Hw=1 for depth values of the slip surface (D) varying from 10 to 100 m computed by the infinite slope model..

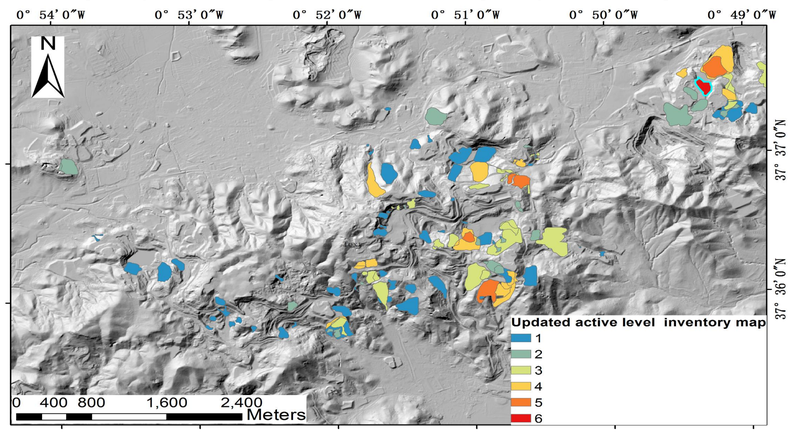

Fig. 7. Distribution of updated active level number inventory map.

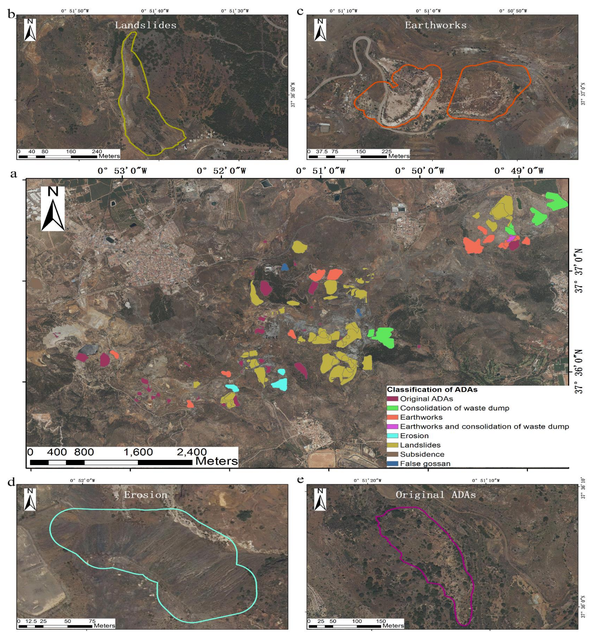

Fig 8. (a) Classification of the different ADA according to the expected underlying deformational process. (b-f) Landslides, earth work, erosion and original ADAs in optical images.

Table 1. Confusion matrix of the number of overlaps between ADA.

	Number of overlapping ADAs					
	Original inventory map	ADA_D	ADA_A	ADA_H	ADA_V	ADA_L
Original inventory map	82	16	19	5	9	12
ADA_D	17	22	14	3	8	5
ADA_A	34	17	34	5	12	12
ADA_H	12	5	9	5	4	5
ADA_V	31	13	16	4	13	8
ADA_L	18	4	9	3	4	35
SF < 1 (H_W =0, D=10 m)	13	3	7	2	5	13
SF < 1 (H_W =1, D=10 m)	13	3	7	2	5	13
SF < 1 (H_W =0, D=100 m)	58	13	20	4	9	22
SF < 1 (H_W =1, D=100 m)	58	14	20	4	9	22

Table 2. Confusion matrix of rate of overlapping ADAs.

	Rate of overlapping ADAs (%)					
	Original inventory map	ADA_D	ADA_A	ADA_H	ADA_V	ADA_L
Original inventory map	100.00	72.73	55.88	100.00	69.23	34.29
ADA_D	20.73	100.00	41.18	60.00	61.54	14.29
ADA_A	41.46	77.27	100.00	100.00	92.31	34.29
ADA_H	14.63	22.73	26.47	100.00	30.77	14.29
ADA_V	37.80	59.09	47.06	80.00	100.00	22.86
ADA_L	21.95	18.18	26.47	60.00	30.77	100.00
SF < 1 (H_W =0, D=10 m)	15.85	13.64	20.59	40.00	38.46	37.14
SF < 1 (H_W =1, D=10 m)	15.85	13.64	20.59	40.00	38.46	37.14
SF < 1 (H_W =0, D=100 m)	70.73	59.09	58.82	80.00	69.23	62.86
SF < 1 (H_W =1, D=100 m)	70.73	63.64	58.82	80.00	69.23	62.86

Table 3. Statistical distribution of type of phenomena causing displacements.

Phenomena	Number	Number of different type phenomena found from ADAs					
		Original inventory map	ADA_D	ADA_A	ADA_H	ADA_V	ADA_L
Original inventory map	40	40	0	0	0	0	0
Consolidation of waste dump	6	1	3	4	0	5	3
Earthworks	12	1	0	3	0	0	12
Earthworks and consolidation of waste dump	2	2	0	0	0	2	2
Erosion	3	0	0	0	0	0	3
Landslides	68	46	23	47	19	33	29
Subsidence	1	0	0	1	0	0	1
False gossan	3	2	0	0	0	2	1

DISCUSSION

To evaluate the performance of the different ADAs, the confusion matrix was calculated using the overlapping accuracy statistics among the original inventory map, the area exhibiting a safety factor lower than 1 (i.e. the unstable areas) in the condition of four extreme values (i.e. H_W =0, D=10 m, and H_W =1, D=10 m, and H_W =0, D=100 m, and H_W =1, D=100 m) and the five types of ADAs (that is ADA_D, ADA_A, ADA_H, ADA_V and ADA_L). According to the six identified ADA maps and safety factor results and the confusion matrices, plus some ancillary information as optical images and the geological map, the ADAs were classified into different types of deformational phenomena (Figure 8 and Table 3). As shown in Figure 8b-f, the optical images of typical phenomena were displayed.

CONCLUSIONS

- A total of 22, 34, 5, 13 and 35 ADAs of ADA_D, ADA_A, ADA_H, ADA_V and ADA_L were identified
- The range of instability increases with the values of D and H_W
- Both InSAR and LiDAR are effective techniques to find ADAs, LiDAR can play a significant in the detection of quick active movement.

ACKNOWLEDGEMENTS

This research was funded by the ESA-MOST China DRAGON-5 project (ref. 59339) and by a Chinese Scholarship Council studentship awarded to Liuru Hu (Ref. 202004180062).

The Sentinel-1A data used in this study were freely downloaded from Copernicus and ESA, and the DEM data is freely downloaded from the website https://centrodedescargas.cnig.es/CentroDescargas/index.jsp. The LiDAR data and orthophotos used in this work were freely downloaded by the Centro Nacional de Información Geográfica (CNIG) del Instituto Geográfico Nacional (IGN) de España (https://www.cnig.es/). The authors would like to thank Dr. Joaquín Mulas from the Instituto Geológico y Minero de España (IGME) for providing a technical report of the study area.